

WFC3-IR Thermal Vacuum Testing: IR channel linearity (flat field illumination – SMS IR04)

M. Robberto (ESA/STSI) & B. Hilbert (STScI)

Abstract

Using a set of RAPID ramps taken during the 2004 WFC3 Thermal Vacuum campaign, we have analyzed the non-linearity of FPA64 under flat-field illumination. The data show that the departure from linearity is similar to the one measured at DCL and complies with CEIS 4.8.8. We parameterize the departure from linearity using a cubic polynomial with constraints allowing to consider only the two higher order coefficients. The distribution of these coefficients shows that they are typically constrained into a relatively narrow range of values, allowing to easily flag out bad pixels. For the large majority of pixels, the two parameter fit provides an excellent fit to their non-linearity as measured by the reduced χ^2 . This should allow for a robust linearity correction. We also analyze in detail the behavior of a bad pixel, selected on the basis of its anomalous non-linearity parameters, finding evidence for exceedingly high forward dark current when saturation is reached in the photon dominated regime. Finally, we define a method to implement linearity correction on actual data.

1. Introduction

Infrared detectors are known to be intrinsically non-linear and the correction for this effect represents one of the major steps in the calibration of raw data. During the 2004 thermal vacuum testing of WFC3 a set of measures has been performed to evaluate the non-linearity and build a preliminary calibration procedure. In this document we report the results relative to the SMS IR04, where the detector linearity has been estimated using flat field illumination.

2. Detector non-linearity

The intrinsic non-linearity of IR detectors derives from the change of junction capacitance with the signal accumulation. The charge Q produced by a pixel of capacitance C is given by

$$Q = C \times V \quad (1.1)$$

where V is the voltage across the detector junction and changes due to the photo generation of free carriers. The pixel capacitance C is the sum of several contributions but is normally dominated by the one of the diode junction, which is a function of the bias voltage and therefore also changes during the integration. The associated flow of current, I_{det} , is given by the change of charge over time:

$$\begin{aligned} I_{\text{det}} &= \frac{dQ}{dt} \\ &= C \frac{dV}{dt} + V \frac{dC}{dt} \\ &= C \frac{dV}{dt} + V \frac{\partial C}{\partial V} \frac{dV}{dt} \\ &= \left(C + V \frac{\partial C}{\partial V} \right) \frac{dV}{dt} \end{aligned} \quad (1.2)$$

which can be rewritten as

$$\frac{dV}{dt} = \frac{I_{\text{det}}}{C + V \frac{\partial C}{\partial V}} \quad (1.3)$$

Equation (1.3) describes the voltage discharge of the detector with time and can be integrated once the detector current I_{det} and capacitance C are known. In general, I_{det} will be the sum of a signal (photocurrent) I_{ph} and a dark (or leakage) current I_{DC} term. The former is simply given by $I_{\text{ph}} = e\eta\Phi$, where e is the charge of the electron, η is the quantum efficiency and Φ is the photon flux. The dark current term is, neglecting tunneling, surface effects and other anomalies, due to two main sources: the diffusion of carriers generated out of the depletion region (diffusion current, I_{diff}) and the generation-recombination of carriers generated within the depletion region (generation-recombination current, I_{GR}). The diffusion current depends on various parameters like the concentration, the mobility and the lifetime of the carriers but has a rather weak dependence on the detector bias. Vice versa, the GR current depends strongly on the detector bias. In what concerns the junction capacitance, is simply given by the standard relation

$$C_{\text{jn}} = \frac{\epsilon A_{\text{pix}}}{W}$$

where ϵ is the dielectric constant of the material, A_{pix} is the area and W is the width of the depletion region, which depends on both the material composition and bias.

We shall not enter here into further details, postponing to a future document a more detailed analysis of the WFC3 IR detectors. We will just notice that in principle the same detector under a dark- or photo-current dominated regime may present different discharge curves. This because a dark-current dominated detector will reach a saturation level at zero bias, whereas a photo-current dominated detector will “overshoot” into the positive bias region. A positively biased diode generates a forward dark current, in the opposite direction to the dark current seen in reverse bias and opposite to the photo-current.

At some point the forward dark current and the photo current balance and the detector remains fixed at the corresponding forward bias, reaching an apparent saturation level. This saturation level depends on the intensity of the photo current, i.e. on the brightness of the source. The dependence, however, is logarithmic and the classical definition of well depth:

$$\text{well depth} = \frac{C \times V}{q}, \quad (1.4)$$

which can be derived from Eq. (1.3) under the assumption of constant capacitance, still represents a good approximation.

3. DCL tests

Figure 1 shows the results of the linearity tests originally performed at DCL on the flight detector, FPA64. The curve indicates that the detector response remains within 5% from linear up to $\sim 97,000$ electrons, and then rapidly saturates at $\sim 110,000$ electrons. The detector enters the forward bias region at $\sim 62,000$ electrons, estimated combining the measured pixel capacitance $\sim 40\text{pF}$ with the operational 0.25V bias.

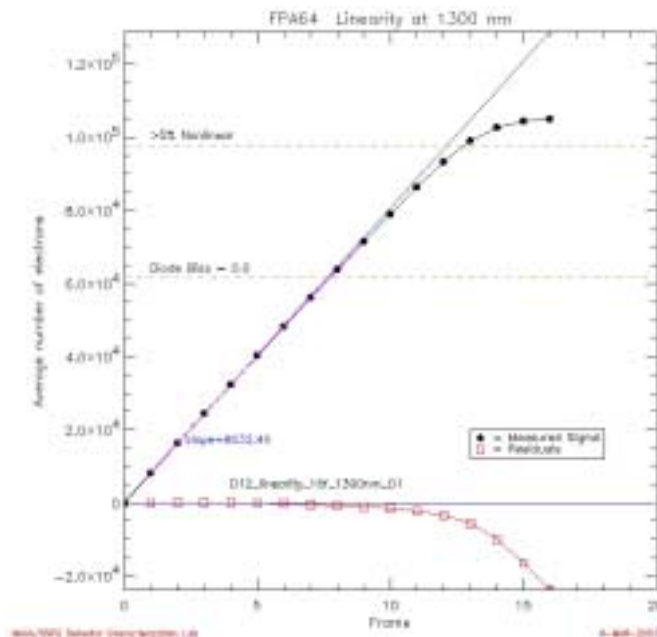


Figure 1: Results of the linearity tests performed at DCL.

4. SMS IR04

Originally, the main goal of this test was to verify that the IR flight detector meets the CEI specifications for linearity. There are two applicable CEIS requirements:

- **CEIS 4.8.7:** “the full well capacity shall be a minimum of 100,000 electrons/pixel with a goal of 150,000 electrons”
- **CEIS 4.8.8:** “the response shall be linear with input signal to <5% (correctable to <0.3%) over the range 100 to 70,000 electrons and independent on exposure time.

The main parameter to be measured was therefore the well-depth at the onset of the non-linearity.

A secondary goal was to build a linearity correction for each pixel of the detector, measuring the response curve through the non-linear regime up to saturation. For this reason this test uses *flat field images*.

Given the limited amount of available time and the focus of the 2004 Thermal Vacuum campaign on functional and performance assessment rather than on calibration, we limited this tests to a preliminary confirmation of the linear regime and to the identification of pixels that may significantly depart from linearity at relatively low count levels.

The measures were done with gain setting = 2.5 e⁻/adu at nominal temperature, T_{det}=150K. The flat field was delivered by an external integrating sphere (i.e. in the CASTLE) fed by IR fibers coupled to a monochromator in single mode (125nm) centered on 1250 nm. The physical slit width was 1500 microns. All of the data were taken at this wavelength and through the WFC3 F125W filter, since no wavelength dependence of the linearity was expected. The CASTLE setup included the neutral density filter ND2 in the filter wheel 1 and open in the filter wheel 2. The predicted count-rate was 1,300 photons/pixel/sec, or ~86,000 in 66 seconds. This total flux puts the detector in forward bias while avoiding over illumination that would trigger detector instability.

The SMS performed a set of 10 ramps bracketed by an initial and a final dark frame. The following tables summarize the main parameters

Table 1 – Main parameters of SMS-IR04

Gain	Exposure time	N _{Exp}	Parameters
2.5 e ⁻ /adu	RAPID = 66.5 secs	10	T = 150K

5. Analysis and test results

The raw data were processed through the standard IR pipeline written in IDL (Hilbert, 2004). An average zero level estimated from the onboard reference pixels was first subtracted from the science pixels. Then the first (zero) read of each ramp was subtracted from each subsequent read to remove pixel-to-pixel bias differences and KTC noise. Spurious values (“cosmic rays”) were removed by analyzing and deglitching the signal of

each pixel up the ramp, and hot/dead pixel masks were also created. The processed data are listed in Table 2, where each file represents a ramp of 15 differential read. The corresponding linear slopes were also organized in individual fits file (with suffix MASKED_FINALIMAGE), and provide a direct image of the flat field response of the detector during the tests.

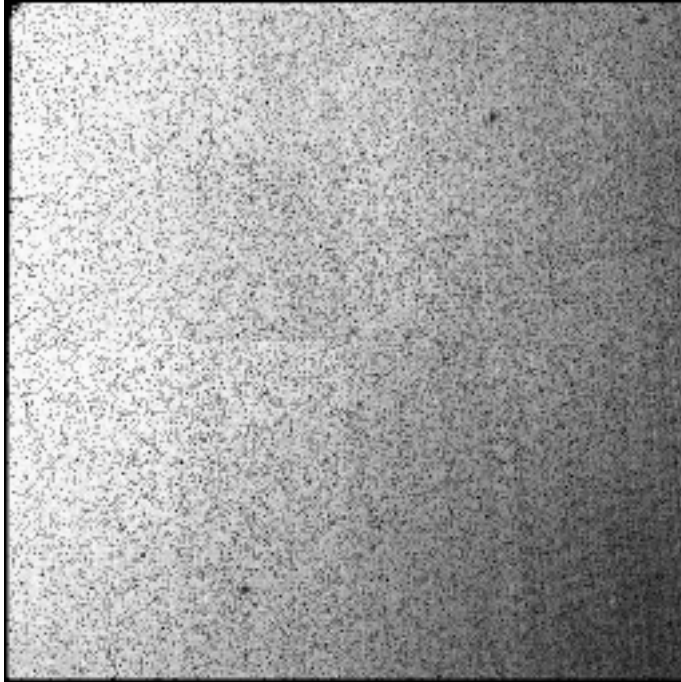
Table 2 – File type and names

Type	Filename
Dark	z.rev.ii040101r_04265085503_raw_opus_subtr_cr_MASKED.fits
RAPID	z.rev.ii040102r_04265085503_raw_opus_subtr_cr_MASKED.fits
RAPID	z.rev.ii040104r_04265091143_raw_opus_subtr_cr_MASKED.fits
RAPID	z.rev.ii040105r_04265091143_raw_opus_subtr_cr_MASKED.fits
RAPID	z.rev.ii040107r_04265092823_raw_opus_subtr_cr_MASKED.fits
RAPID	z.rev.ii040108r_04265092823_raw_opus_subtr_cr_MASKED.fits
RAPID	z.rev.ii04010ar_04265094503_raw_opus_subtr_cr_MASKED.fits
RAPID	z.rev.ii04010br_04265094503_raw_opus_subtr_cr_MASKED.fits
RAPID	z.rev.ii04010dr_04265100143_raw_opus_subtr_cr_MASKED.fits
RAPID	z.rev.ii04010er_04265100143_raw_opus_subtr_cr_MASKED.fits
RAPID	z.rev.ii04010gr_04265101857_raw_opus_subtr_cr_MASKED.fits
Dark	z.rev.ii04010hr_04265101857_raw_opus_subtr_cr_MASKED.fits

As an example, we show in Figure 2 the flat field image obtained from the first RAPID ramp, i.e. the file

z.rev.ii040102r_04265085503_raw_opus_subtr_cr_MASKED_FINALIMAGE.fits

The detector illumination is clearly non uniform, as the signal varies by ~10% across the array. In Figure 3 we show for comparison the flat field image at 1.0 μm obtained at DCL (available at the DCL/WFC3 SOC page). The similarity between the two images indicates that the non uniformity is intrinsic to the device and not due to illumination effects. Note that we had to rotate the DCL image by 90 degrees clockwise to obtain the same orientation of the frames delivered by the pipeline.



2	3
1	4

Figure 2: Flat field image obtained during the thermal vacuum tests

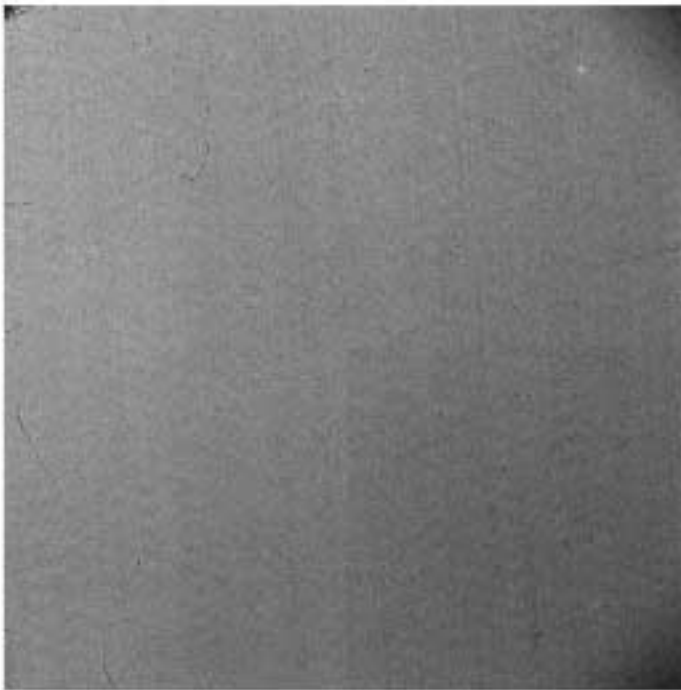


Figure 3: Flat field image obtained by DCL

6. Average linearity of each quadrant

A first analysis of the linearity can be performed by looking at the average signal during the ramps. We have independently considered the four quadrants, plotting for each read the corresponding histogram of the counts. In Figure 4 we show the results for the 4 quadrants, still relative to the first RAPID ramp. Each series of "bells" represents a quadrant (see the insert in Figure 2 for the location of each quadrant). For clarity, the frequencies (nr. of pixels) are plotted in Figure 4 with no offset (quadrant 1), and with a 3000, 6000 and 9000 offset for quadrants 2, 3 and 4, respectively. The signal, converted to electrons using the nominal 2.5e/adu gain, increases from left to right following the integration. At each read the distribution becomes broader and the peak less pronounced due to the increase of shot noise; at each read the four quadrants have a signal offset that reflects the flat field response, e.g. quadrant 2 is the brightest and quadrant 4 is the dimmest.

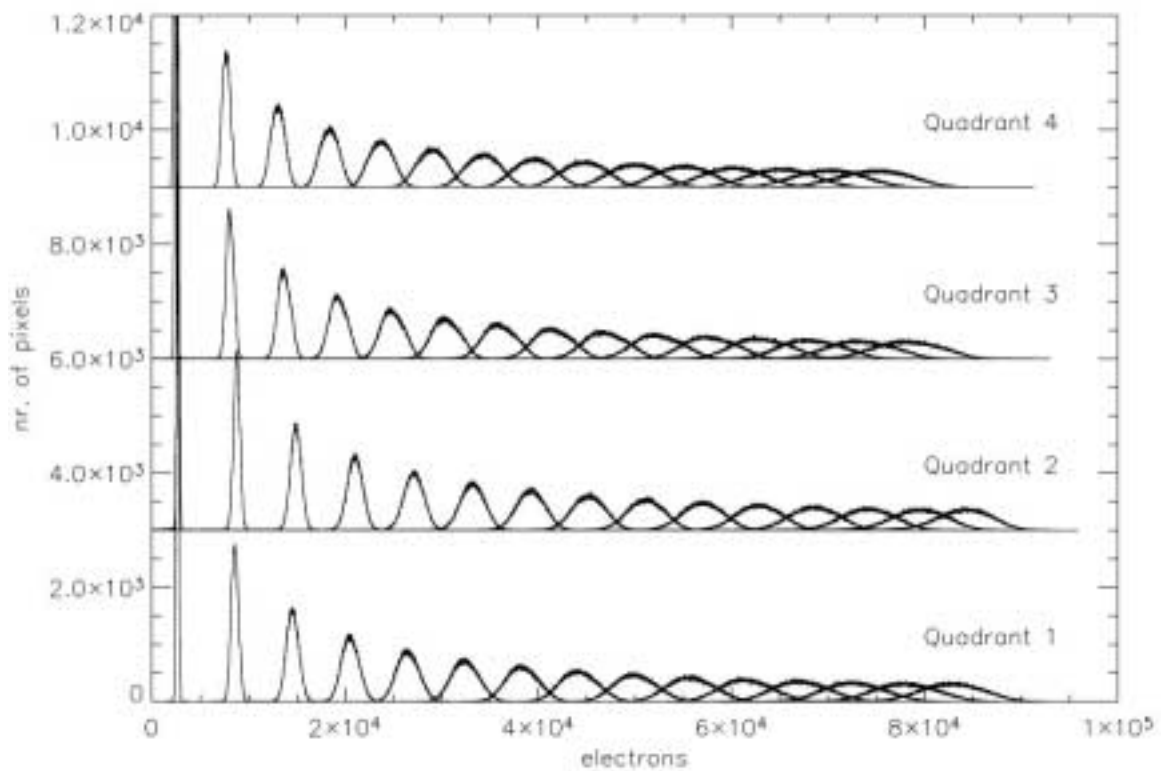


Figure 4: Histograms of the signal response for the 4 quadrants during the first RAPID ramp (see text).

A gaussian fit to each "bell" allows an accurate estimate of the average signal and standard deviation of the distribution. In Table 3 we report the values corresponding to the ramps we are considering.

Table 3: mean and standard deviation of the signal plotted in Figure 4.

	Quadrant 1		Quadrant 2		Quadrant 3		Quadrant 4	
Read	Mean	Stdev	Mean	Stdev	Mean	Stdev	Mean	stdev
1	2634.96	124.383	2694.64	109.818	2479.81	132.17	2364.84	142.133
2	8580.14	378.459	8785.72	328.637	8070.37	404.789	7695	435.907
3	14548.2	639.629	14905.2	555.921	13676.1	678.558	13040.5	725.121
4	20518.5	903.643	21026.8	786.195	19280.3	952.929	18387.8	1010.23
5	26473.7	1168.13	27129.8	1017.56	24867.5	1224.26	23718	1290.88
6	32403.2	1431.38	33203.3	1249.15	30430.9	1492.08	29028.7	1565.94
7	38300.9	1692.35	39238.3	1477.73	35962.9	1755.4	34310.3	1835.68
8	44162.2	1950.7	45230.2	1704.05	41460.1	2016.82	39562.7	2100.6
9	49984.5	2205.27	51172.1	1925.47	46918.8	2273.09	44781.8	2361.56
10	55758	2450.19	57053.6	2138.85	52336.5	2521.73	49967.8	2618.88
11	61472.6	2692.37	62864.4	2351.47	57697.9	2761.4	55105.5	2863.26
12	67113.5	2928.62	68584.6	2554.14	62992.7	2995.93	60184.1	3099.14
13	72648.2	3142.37	74171.9	2736.84	68209.1	3221.11	65199.9	3326.86
14	78005.6	3288.42	79523.6	2818.35	73316.1	3420.91	70130.9	3532.1
15	82843.1	3257.69	84247.2	2758.5	78260.6	3495.46	74951.2	3683.58

The plot of the mean counts vs. read number for each quadrant provides a first look into the detector non-linearity. In Figure 5 we show the results relative to the first ramp. The linear fit has been estimated using the first 7 read, a rather arbitrary value chosen on the assumption that most of the non-linearity will show up in the forward bias regime. The residuals, estimated as difference between the straight line fit and the measured values for display purposes, is also plotted. It has been multiplied by 10 for visualization purposes.

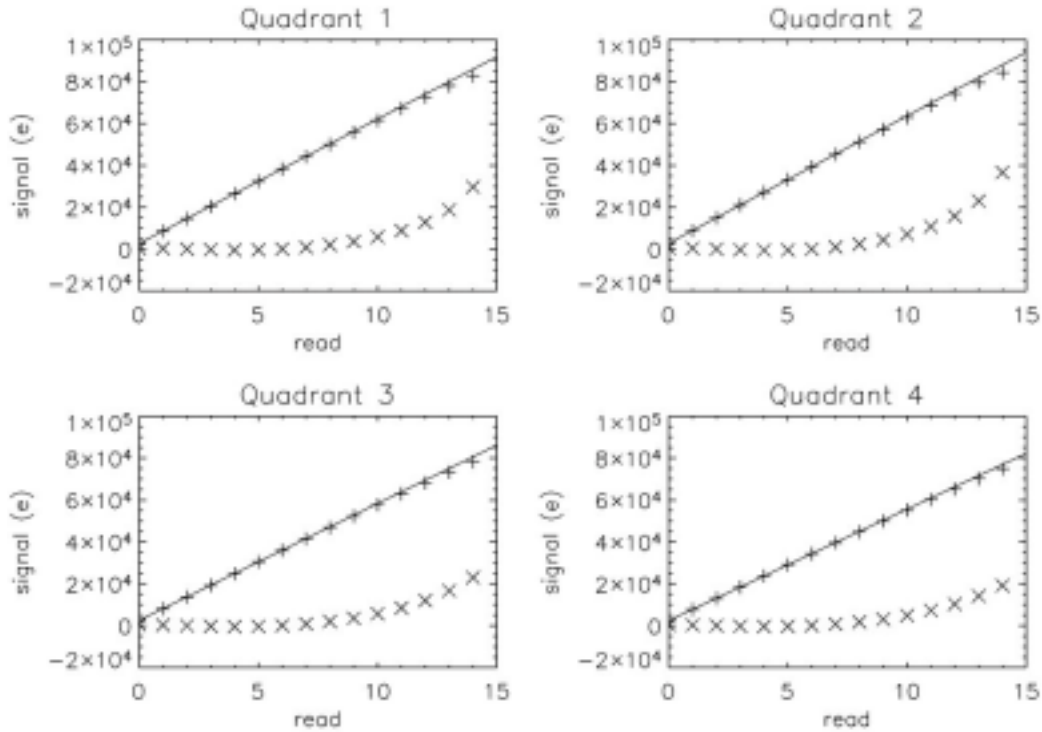


Figure 5: Average signal for each quadrant. The dotted line represents the residual, multiplied by 10.

Figure 5 indicates that the detector remains well within 5% of linear within the entire range of accumulated charge we have considered, ~83000 electrons. This is in agreement with the previous measures of DCL (Section 3). The brightest quadrants 1 and 2 also display the highest non-linearity, as expected.

All other 9 ramps with flat field illumination show very similar results.

It is interesting to compare the dark current frames taken before and after the sequence of illuminated ramps. Figure 6 shows a significant change between the dark current frames taken at the beginning and at the end of the illumination, a clear indication of a persistency effect in the detector.

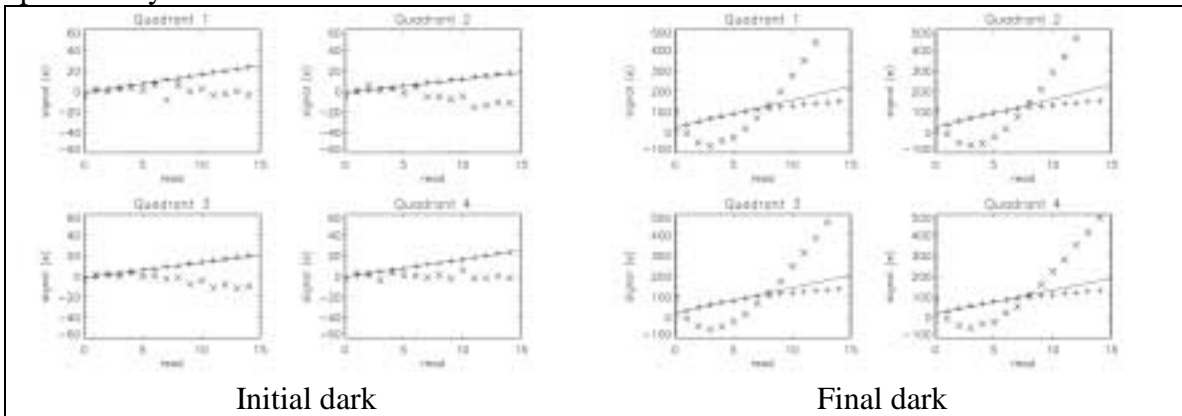


Figure 6: dark current ramps taken at the beginning and at the end of the SMS. The scale is the same for both images.

7. Linearity of individual pixels

In Figure 7 we show the data relative to four randomly selected pixels on quadrant 1. Each ramp represents one pixel, from the bottom to the top: pixel [100,100], [100,200], [100,300] and [100,400]. To the last three pixels we have added an offset of 10,000, 20,000 and 30,000 electrons respectively for display purposes. Let's concentrate on pixel [100,100], i.e. the bottom ramp. For each signal level there are 10 crosses, the read values obtained during the 10 repeats of the sequence. The first cross of each group therefore represents the first ramp, and so on. Note that the first ramp appears to be always lower than the other 9, and this is generally true also for the other pixels. The first ramp, therefore, has lower counts than all the following ones, another proof that the detector behaves differently depending on the illumination history. Previous illumination gives higher signal, a memory effect we normally refer to as "persistence".

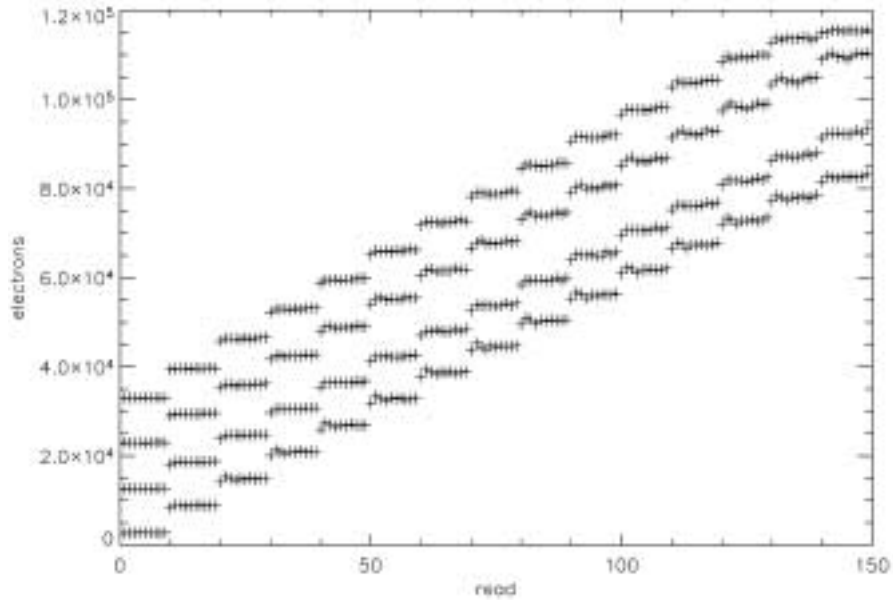


Figure 7: Values obtained in 10 RAPID ramps for four pixels (see text).

To analyze the behavior of each pixel one can average the 10 reads to obtain a more robust estimate of the signal, possibly neglecting the first read immediately following the reset. We thus obtain a cube of $15 \times 507 \times 507$ mean values per quadrant. Ideally, each pixel should behave according to the mean average response discussed in the previous section. We can repeat the same type of analysis fitting a stray line to the first part of the curve of each individual pixels. To be slightly more conservative we use in this case the first 6 reads, performing a fit to the first 5 differences (read 1 to 6 minus read 0). The residuals, similar to those presented in Figure 6, can be fit using a 3rd order polynomial. We force the polynomial to have zero value and null derivative at the origin, to be consistent with a ramp that starts linearly from the origin. The fit to the residuals is therefore given by the equation

$$y = Ax^2 + Bx^3. \quad (1.5)$$

We can therefore use two parameters to characterize the non-linearity: A, the quadratic one, describes the parabolic shape of the curve, whereas B, the cubic one, describes the higher order departure from a parabola.

Figure 8 shows the fit for our randomly selected pixel (100,100).

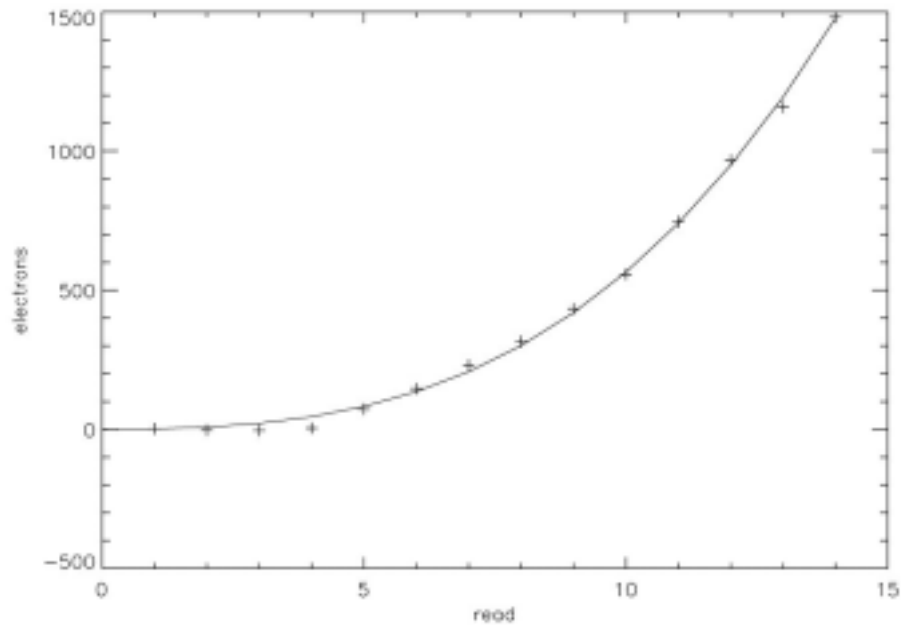


Fig.8: 3rd order polynomial fit to the non-linearity of pixel (100,100). The values of the Coefficient of Eq. (1.5) are A=0.914 and B=0.473.

Having described the non-linearity with two parameters, we can explore their distribution to find anomalous pixels. The locus of the A, B parameters for the first quadrant is shown in Figure 9. The large majority of pixels is distributed along a “main sequence” limited by A=[-70,0] and B=[0,10]. The presence of A vs. B relation is most probably a result of the functional relationship described by Eq. (1.3). Note that the A values are typically negative, giving a parabola with a maximum at the origin. The cubic term is therefore dominant and the one who turns upward the concavity of the curve. It is clear from Figure 9 that there are, however, pixels well outside of the sequence, in particular with values up to A~1000.

In Figure 10 we show the ramp of one of these anomalous pixels (i=269, j=104), indicated by the red circle in Figure 9, which has A=1088.62 and B=-45.02, . The ramp starts with a large slope and then saturates at approximately 42,000 electrons. For comparison, we show in Figure 10 the ramps for the 8 adjacent pixels. They behave normally, thus the defect at least in this case is entirely confined to one pixel.

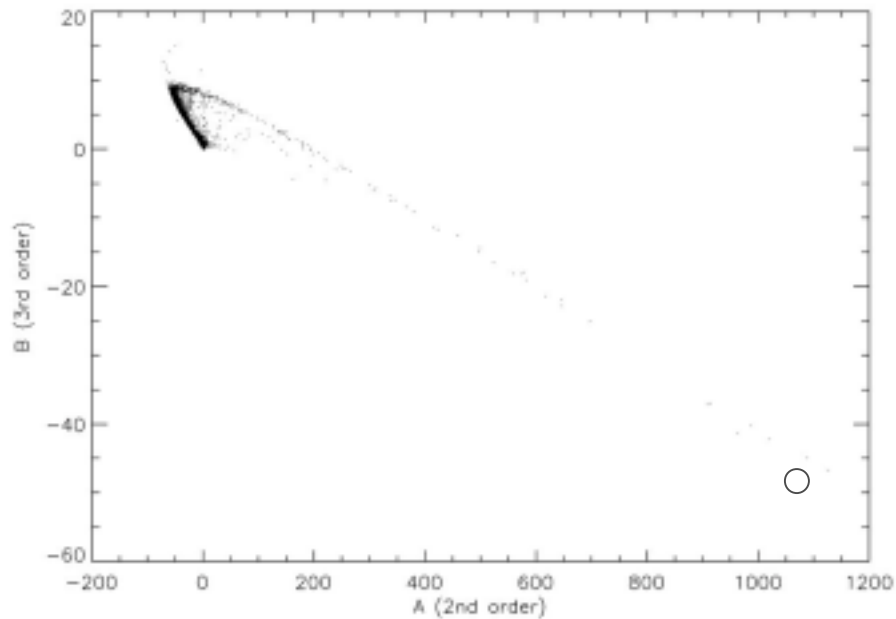


Figure 9: Locus of the values of the coefficients A and B describing the departure from linearity for all the active pixels of quadrant 1 (5:511,5:511)

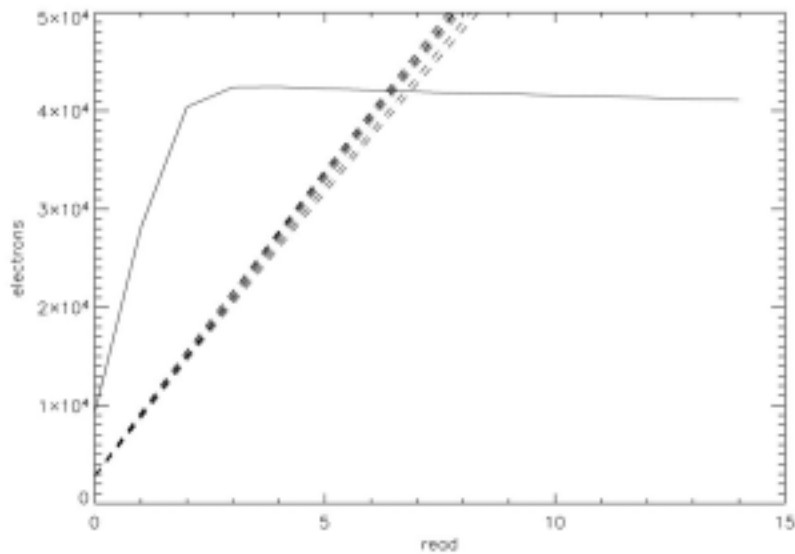


Figure 10: Signal ramp for the anomalous pixel $i=269, j=104$ (solid line) and for the 8 adjacent pixels (dashed line).

The main difference between a pixel like (269,104) and the nearby ones is therefore the extremely high rate before reaching saturation, rather than the saturation level itself. A saturation level at $\sim 40,000$ electrons would be acceptable in the majority of cases, but here we are in the presence of an anomalous short transient response, associated with an exceedingly high forward dark current. This is shown in Figure 11, which compares the 10 ramps with light on to the two dark current ramps. After read nr. 3 the dark current dominates over the signal. The zero bias (dark current dominated) saturation level is nicely flat at 44,000 electrons. In photo-current dominated mode (light on) the detector

should overshoot in the forward bias regime, but apparently the induced forward bias dark current is so strong that actually “recharges” the junction causing a net decrease of the signal. Pixels like (269,104) cannot be recovered, they must be flagged out and rejected by bad pixel masking.

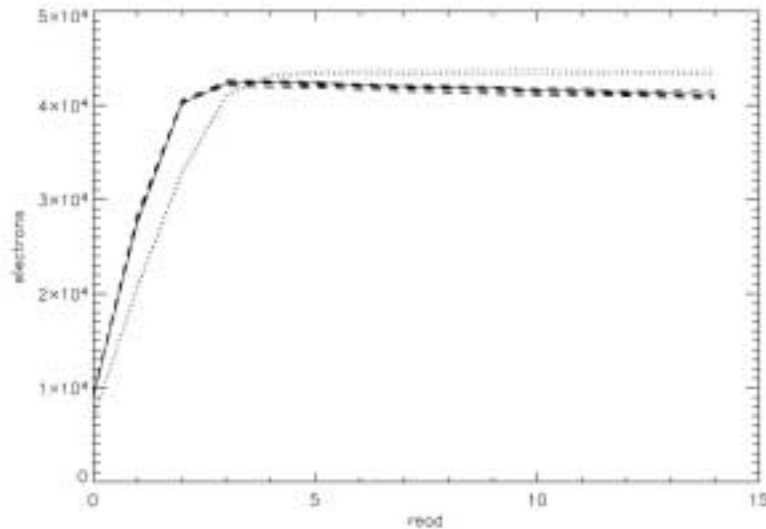


Figure 11: The ramps for the a bad pixel, (269,104) of quadrant one, with flat field illumination (dashed lines) and pure dark before and after illumination (dotted lines).

For the majority of pixels, the A and B parameters should allow for a good linearity correction. But how much good? To give a quantitative answer to this question we have estimated, for each pixel in quadrant 1, the reduced χ^2 of the fit to the *average* ramp, obtained from the 10 ramps with light on. The histogram of the results is plotted in Figure 11. The great majority of pixels fall within the main peak of small χ^2 values, i.e. they have a good fit. Pixels with small χ^2 actually have A and B values falling in a rather restricted range. This is shown in Figure 12, which is similar to Figure 9 with at zoom in at the origin of the axes, except that this time we have selected only pixels with $\chi^2 < 0.2$.

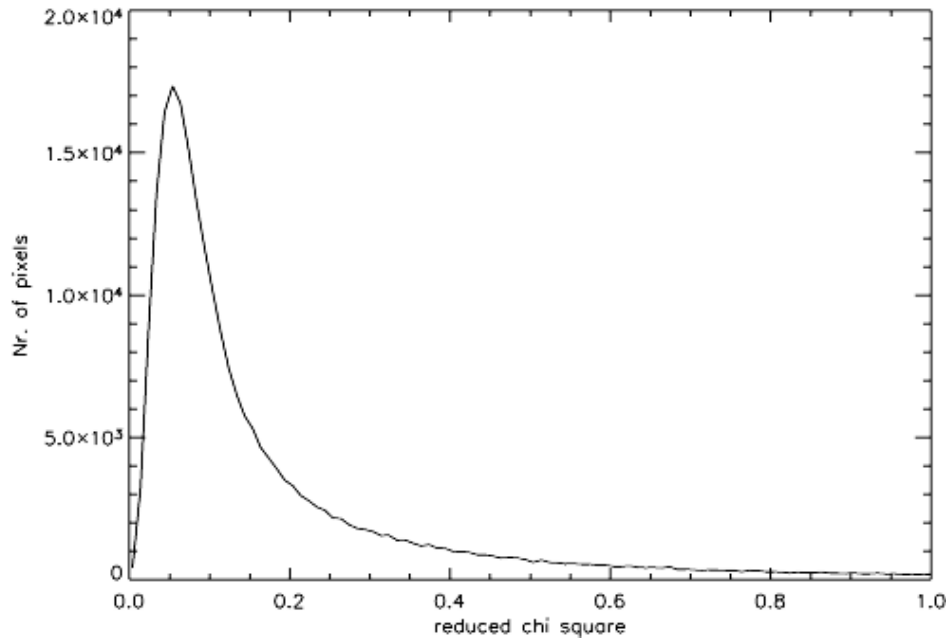


Figure 11: Histogram of the reduced chi-square of the fits to the non-linearity curves of pixels in quadrant 1.

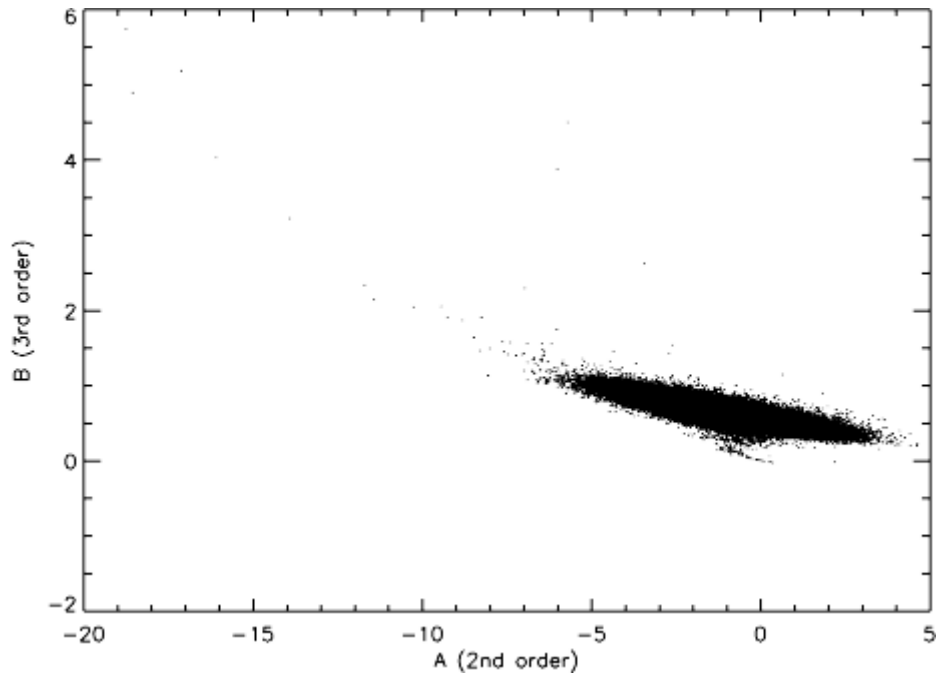


Figure 12: Same as Figure 9, but for pixels having $\chi^2 < 0.2$.

8. Toward an explicit non-linearity correction

In this last part we will derive an explicit equation to correct for the detector non-linearity, based on the 10 flat-field ramps considered in the previous sections. Since the goal of the Thermal Vacuum campaign was not to obtain calibration data but rather to explore the detector behavior, we do not pretend to create a *final* calibration file but rather to explore a method. Still, the calibration file we are going to derive should provide a significant improvement over uncorrected data and shed some more information on the detector characteristics.

Our procedure, implemented by the IDL code attached in the Appendix, follows the following steps:

1. After having read the 10 ramps, we build a super-ramp taking, for each pixel [i,j] and read (n=1...15), the median of the 10 values provided by each ramp. Remember that the ramps are processed, i.e. the first read is subtracted from all subsequent reads. Thus, when we say 15 “read” we actually mean 15 differences created from the original 16 read.
2. For each pixel, we produce a linear fit to the first 6 read. In our real implementation, we have actually discard the first read (difference 1-0).
3. With the linear fit parameters, we calculate for each pixel the linearized value corresponding to the each read.
4. To avoid fitting saturated values, we check that the increment between successive ramp read are not too low. This because due to non linearity the increment becomes more and more and saturation corresponds to increments close to 0. In practice, we require that the increment must remain larger than half of the rate measured at the very beginning of the ramp (excluding the first read, i.e. difference 2-1). All values satisfying this criterion can be linearized.
5. The ratio between the linearized and the original value provides the correction curve. It will be close to 1 at the low flux levels and larger than 1 at high flux levels.
6. We fit the correction curve with the same polynomial fit discussed in the previous section, with two differences: we subtract 1 from the correction curve in order to use the same expression with constant term equal to 0, and we use as independent variables the read/difference values instead of the order nr. 1 to 15 used in the previous section. We also limit ourselves to the good reads that show increment larger than half of the initial one. The factor of 1 has to be added again in the final correction equation, i.e. we have this time the expression

$$y = x(I + A'x^2 + B'x^3) \quad (1.6)$$

where x are the signal counts actually detected by the pixel

In conclusion, we derive 4 parameters

- The 2nd and 3rd order coefficient of the polynomial fit A' and B' ;
- The Highest Corrected Value used to estimate the fit (higher values correspond to rates lower than ½ the initial rate);
- A percentile departure from linearity at the Highest Corrected Value, which can be regarded as a measure of the residual error remaining after applying the linearity correction.

The results contained in the file *lin_cal.fits*. Figure 13, similar to Figure 9 and 12, shows the locus of the new A' and B' parameters, whereas Figure 14a-d shows the spatial distribution of the four linearization parameters. The Highest Corrected Value ranges between 28,000 and 40,000 counts, whereas the percentile departure after correction is typically less than 0.1%.

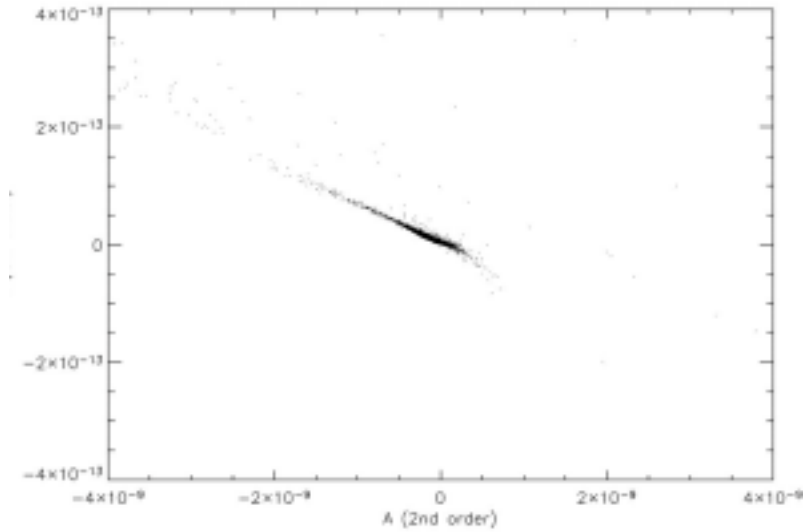


Figure 13: Same as Figure 9 and 12, for the effective linearization parameters.

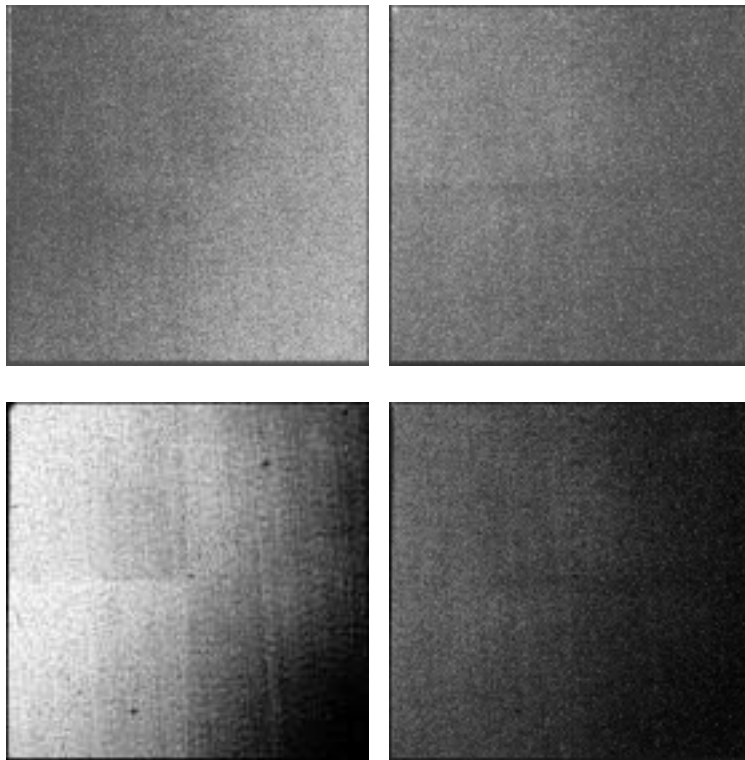


Figure 14: Spatial distribution of the linearization parameters: a) top-left: A' ; b) top-right: B' ; c) bottom-left: Highest Corrected Value; d) bottom right: percentile residual from linearity.

9. Conclusion

Using a set of data taken during the 2004 WFC3 Thermal Vacuum campaign, we have analyzed the non-linearity of FPA64 under flat field illumination. The data show that the departure from linearity is similar to the one measured at DCL and complies with CEIS 4.8.8. We parameterize the non-linearity using a cubic polynomial, with added constraints allowing us to consider only the two higher order coefficients. For the large majority of pixels, these coefficients are distributed into a relatively narrow range of values and provide an excellent fit to their non-linearity, measured using a reduced χ^2 . Bad pixels clearly appear as outliers with respect to the main distribution of parameters. We analyze in detail the behavior of one of the bad pixels finding evidence for exceedingly high forward dark current when saturation is reached in the photon dominated regime. Finally, we define a method to implement linearity correction on actual data.

APPENDIX

```
pro lin_cor
;This routine estimates the non linearity of the pixels
;vs. signal, not vs. readnumber. It is therefore better suited
;to correct for the linearity
frame = fltarr(10,16,1014,1014)
Superamp=fltarr(16,1014,1014)
;select Active area only
x0=5
x1=1018
y0=5
y1=1018
;
;READ THE RAMPS, NO DARKS
PATH = 'D:\WFC3 data\IR04S01\'
for i=0,14 do begin
;fits_read,PATH+'z.rev.ii040101r_04265085503_raw_opus_subtr_cr.fits',a,EXTEN_NO=i+1 ;#0
fits_read,PATH+'z.rev.ii040102r_04265085503_raw_opus_subtr_cr.fits',a,EXTEN_NO=i+1 ;#1
frame(0,i,*,*)=a[x0:x1,y0:y1]
fits_read,PATH+'z.rev.ii040104r_04265091143_raw_opus_subtr_cr.fits',a,EXTEN_NO=i+1 ;#2
frame(1,i,*,*)=a[x0:x1,y0:y1]
fits_read,PATH+'z.rev.ii040105r_04265091143_raw_opus_subtr_cr.fits',a,EXTEN_NO=i+1 ;#3
frame(2,i,*,*)=a[x0:x1,y0:y1]
fits_read,PATH+'z.rev.ii040107r_04265092823_raw_opus_subtr_cr.fits',a,EXTEN_NO=i+1 ;#4
frame(3,i,*,*)=a[x0:x1,y0:y1]
fits_read,PATH+'z.rev.ii040108r_04265092823_raw_opus_subtr_cr.fits',a,EXTEN_NO=i+1 ;#5
frame(4,i,*,*)=a[x0:x1,y0:y1]
fits_read,PATH+'z.rev.ii04010ar_04265094503_raw_opus_subtr_cr.fits',a,EXTEN_NO=i+1 ;#6
frame(5,i,*,*)=a[x0:x1,y0:y1]
fits_read,PATH+'z.rev.ii04010br_04265094503_raw_opus_subtr_cr.fits',a,EXTEN_NO=i+1 ;#7
frame(6,i,*,*)=a[x0:x1,y0:y1]
fits_read,PATH+'z.rev.ii04010dr_04265100143_raw_opus_subtr_cr.fits',a,EXTEN_NO=i+1 ;#8
frame(7,i,*,*)=a[x0:x1,y0:y1]
fits_read,PATH+'z.rev.ii04010er_04265100143_raw_opus_subtr_cr.fits',a,EXTEN_NO=i+1 ;#9
frame(8,i,*,*)=a[x0:x1,y0:y1]
fits_read,PATH+'z.rev.ii04010gr_04265101857_raw_opus_subtr_cr.fits',a,EXTEN_NO=i+1 ;#10
frame(9,i,*,*)=a[x0:x1,y0:y1]
;fits_read,PATH+'z.rev.ii04010hr_04265101857_raw_opus_subtr_cr.fits',a,EXTEN_NO=i+1 ;#11
;ramp1(i,*,*) = a
endfor

;from the 10 repeat of the ramp, make a super-ramp
Superamp=MEDIAN(frame,DIMENSION=1)

;MAKE A fit to read 1 to 6 included. Avoid 0 and
gain=2.5
Nonlin=fltarr(1014,1014)
ABvalues=DBLarr(2,1014,1014)
ChiSquare=fltarr(1014,1014)
Fmax = fltarr(1014,1014)
DeltaM=fltarr(1014,1014)

FOR i=0,1013 do begin ;506
FOR j=0,1013 do begin ; 506
X=Superamp[0:14,i,j]
Xs=Superamp[1:4,i,j] ;FIT ONLY READ 1 to 6
```

```

result=linfit(indgen(4)+1,Xs)

line=result[0]+result[1]*indgen(15)

;SATURATION CHECK
deltaX = ABS(X-shift(X,1))
cutoff = deltaX[1]/2.
good=where(deltaX(1:*) GT cutoff,ngood)
Nmax = 14<ngood
;
curve=line/X
curve=curve[0:Nmax]
;
weights=replicate(1,Nmax+1);X[0:Nmax]
AB=[1.,1.]
IF Nmax GE 2 THEN $
yfit=CURVEFIT(X[0:Nmax],curve[0:Nmax]-
1,weights,AB,SIGMA,CHISQ=C2,FUNCTION_NAME='gfunct',/DOUBLE)

CHISQUARE[i,j]=C2
ABvalues[* ,i,j]=AB
Fmax[i,j] = X[Nmax]
DeltaM[i,j] = (line[Nmax]-X[Nmax]*(AB[0]*X[Nmax]^2+AB[1]*X[Nmax]^3+1))/line[Nmax]*100.

;plot,line,X
;oplot,line,X*curve,linestyle=2
;oplot,line,X[0:Nmax]*(AB[0]*X[0:Nmax]^2+AB[1]*X[0:Nmax]^3+1),psym=5
;print,i,j,DeltaM[i,j]
endfor
endifor

openeps,'C:\Documents and Settings\robberto\My Documents\WFC3\Thermal Vac\IR04-
results\'+Fig20.eps'
plot,abvalues[0,*,*],abvalues[1,*,*],psym=3,xtitle='A (2nd order)',ytitle='B (3rd
order)'xrange=[-s1,s1]/1.E8,yrange=[-s2,s2]/1.E10
closeps

DCUBE = FLTARR(4,1024,1024)
DCUBE[0,5:1018,5:1018]= ABvalues[0,*,*]
DCUBE[1,5:1018,5:1018]= ABvalues[1,*,*]
DCUBE[2,5:1018,5:1018] = FMax
DCUBE[3,5:1018,5:1018] = DeltaM

writefits,'C:\Documents and Settings\robberto\My Documents\WFC3\Thermal Vac\IR04-
results\'+lin_cal.fits',dcube;,HDR;,/extend
;check
;fits_READ,'C:\Documents and Settings\robberto\My Documents\WFC3\Thermal Vac\IR04-
results\'+lin_cal.fits',AAA,HHH

END

PRO gfunct,X,AB,F,pder
F=AB[0]*X^2+AB[1]*X^3
pder=[[X^2],[X^3]]
END

```